Revealing correlated electronic and nuclear dynamics in molecules with energy-resolved population imaging

Kunlong Liu, Pengfei Lan,* Cheng Huang, Qingbin Zhang, and Peixiang Lu†
School of Physics, Huazhong University of Science and Technology, Wuhan 430074, China
(Received 17 February 2014; published 28 May 2014)

We explore a method, named energy-resolved population imaging (EPI), to analyze on an equal footing the temporary electronic transition and nuclear motion during laser-molecular interaction. By using EPI we have intuitively demonstrated the population transfer in vibrational H_2^+ exposed to extreme ultraviolet pulses, revealing the energy-sharing rule for the correlated electron and nuclei. We further show that EPI can be extended to uncover the origins of the distinct energy-sharing mechanisms in multiphoton and tunneling regimes. The present study has clarified a long-standing issue about the dissociative ionization of H_2^+ and paves the way to identify instantaneous molecular dynamics in strong fields.

DOI: 10.1103/PhysRevA.89.053423 PACS number(s): 33.80.Rv, 33.80.Wz, 42.50.Hz

I. INTRODUCTION

The electronic and nuclear dynamics in laser-molecular interaction have been studied extensively due to the potential applications that rely on the underlying mechanisms. The applications include molecular high-order-harmonic generation [1,2], nuclear dynamics detection [3,4], self-imaging of molecules [5], attosecond control of the formation and rupture of chemical bonds [6,7], and so on. Despite more than 20 years of research in this field, the correlated electron-nuclear dynamics in molecules still attracts continuous interest inspired by the unexpected and even counterintuitive phenomena in laser-driven molecular fragmentation [8–11].

The simplest molecule H_2^+, which is accessible to experimental investigations and *ab initio* calculations, has been a prototype object to study strong-field processes of molecules [12]. Typically, the laser-induced fragmentation of the molecule includes two pathways, namely, dissociation and dissociative ionization. For the dissociation pathway, several mechanisms (e.g., bond softening [13] and above-threshold dissociation [14]) have been well identified [12]. For the dissociative ionization, however, two mechanisms, i.e., above-threshold Coulomb explosion [15] and charge-resonance-enhanced ionization [16], were proposed to be responsible for the modulation of the nuclear kinetic-energy-release (KER) spectrum following ionization of H_2^+, leading to a long-standing controversy [15–19]. Many efforts have been made to explain the intermediate process in dissociative ionization of H_2^+ [20–24], but there is still no direct evidence to demonstrate the ionization and nuclear motion on equal footing.

Recently, the joint energy spectrum (JES) has been proposed to analyze the correlated electron-nuclear dynamics in dissociative ionization of molecules [25–28], which is an important step to understand the final energy sharing between the electron and the nuclei. However, the details of how the photon energy is deposited to the fragments *during* the interaction are still unclear. Moreover, it is found that the way for electron and nuclei to share energy in tunnel ionization differs from that in a multiphoton regime [26]. This finding further raises the question, What are the origins of the distinct energy-sharing mechanisms in dissociative ionization of molecules? Since the general physical picture for the unexpected phenomena in molecular fragmentation is somewhat hidden from the observables, an appropriate theoretical representation that helps scientists directly "see" how molecular fragmentation proceeds is desired.

On the one hand, the information about the instantaneous correlated electron-nuclear dynamics in molecular fragmentation is "coded" within the time-dependent Schrödinger equation (TDSE) beyond the Born-Oppenheimer (BO) approximation [29,30]. The wave packets of the correlated electron and nuclei can be obtained by solving the TDSE. However, the wave packets in the space representation can hardly provide meaningful insights into the instantaneous dynamics [31]. On the other hand, the diagram of molecular potential curves was widely used to outline the mechanisms of the molecular fragmentation via illustrating the population transfer. But the description of the population transfer or the nuclear motion is on a qualitative level, and it usually involves speculations based on the observables. Potentially, even for the same experimental phenomena, different speculations would lead to distinct conclusions regarding the responsible mechanisms [15,16], ultimately giving rise to the confusion about the underlying dynamics. Therefore, to demonstrate the underlying molecular dynamics, the most intuitive and direct way would be quantitatively reproducing the time evolution of the population transfer on the potential curves with TDSE solutions. In this paper, we accomplish this by introducing an intuitive representation, named energy-resolved population imaging (EPI), on the basis of a resolvent method [32] that allows for extracting the population of the continuum and the bound states. By using EPI, we have theoretically studied the dissociative ionization of vibrational H_2^+ exposed to extreme ultraviolet (XUV) pulses. By demonstrating the temporary population transfer, we have deduced the rule for respective amounts of the energy taken by the correlated electron and nuclei. We further demonstrate the dissociative ionization in multiphoton and tunneling regimes with the EPIs, intuitively revealing the origins of the distinct energy-sharing mechanisms.

*pengfeilan@hust.edu.cn
†lupeixiang@hust.edu.cn

II. THEORETICAL MODEL

For numerical simulations we solved the TDSE for a reduced-dimensionality model of H_2^+. In this model, the one-dimensional motions of the nuclei and the electron are assumed to remain aligned with the linearly polarized laser field. Even so, this model was widely used to identify the strong-field processes [11,12,25,26] and reproduced the experimental result at least qualitatively [16,30]. Thus, the simplified model of H_2^+ is practical and reliable for studying molecular dynamics in strong field. Within this model, the length-gauge TDSE can be written as (atomic units are used throughout) $i\frac{\partial}{\partial t}\Psi(R,z;t) = [T_N + T_e + V_0 + V_t]\Psi(R,z;t)$, where $T_N = -\frac{1}{m_p}\frac{\partial^2}{\partial R^2}$, $T_e = -\frac{1}{2}\frac{\partial^2}{\partial z^2}$, $V_t = \varepsilon(t)z$, and $V_0 = \frac{1}{R} + V_e(z,R)$, with $V_e(z,R)$ being the improved soft-core potential that reproduces the exact $1s\sigma_g$ potential curve in full dimensions [30]. Here, R is the internuclear distance, z is the electron position measured from the center of mass of the protons, and m_p is the mass of the proton. The laser electric field is given by $\varepsilon(t) = \varepsilon_0 \exp[-2\ln 2(t/\tau)^2]\sin(\omega t)$, with τ being the pulse duration, ω being the central frequency, and ε_0 being the peak electric-field amplitude.

The TDSE is solved on a grid by using the Crank-Nicolson split-operator method with a time step of $\Delta t = 0.04$ a.u. The grid ranges from 0 to 25 a.u. for R and from -1500 to 1500 a.u. for z, with grid spacings of $\Delta R = 0.05$ a.u. and $\Delta z = 0.2$ a.u. To obtain intuitive insights into the temporary molecular dynamics, we now introduce EPIs. An EPI is analogous to diagrams with molecular potential curves and sketched wave-packet profiles but provides a quantitative and accurate description of the population transfer. The general idea of calculating an EPI is to convert the wave function $\Psi(R,z;t)$ at t, or $\Psi_t(R,z)$, to the density distribution $\rho(R,E)$, with E being the potential energy. We have accomplished the conversion by extracting the energy density distribution from the z-dimensional wave function of $\Psi_t(R,z)$ at each internuclear distance. The extraction is based on the resolvent method introduced by Schafer and Kulander [32]. A time-dependent energy window operator is defined by $\hat{W}_t(E,k,\epsilon) = \epsilon^{2k}/[(\hat{H}_t - E)^{2k} + \epsilon^{2k}]$, with $\hat{H}_t = T_e + V_0 + V_t$. The probability density of the energy E at each R can be obtained from

$$\rho(E;R) = \langle\Psi_t(z;R)|\hat{W}_t|\Psi_t(z;R)\rangle/C = \langle\Psi_t(z;R)|\frac{\epsilon^{2k}}{(\hat{H}_t - E)^{2k} + \epsilon^{2k}}|\Psi_t(z;R)\rangle/C, \quad (1)$$

with $C = \epsilon\frac{\pi}{k}\csc(\frac{\pi}{2k})$ [26]. Here we use the parameters $\epsilon = 0.004$ and $k = 2$. Note that the definition of the operator $\hat{H}_t$ is based on the length-gauge TDSE; thus, the EPI is not gauge invariant.

III. RESULTS AND DISCUSSION

Figure 1 shows the simulation results of the correlated electron-nuclear energy spectrum, i.e., the JES, for the interaction of H_2^+ with a 0.8-fs XUV pulse at 30 nm and a peak intensity of 10^{14} W/cm^2. The JES are obtained by using the method from [26]. A number of initial vibrational states ($v = 0$, 2, 5, 11, 13 and 15) of $H_2^+(1s\sigma_g)$ have been chosen, as indicated in the panels of Fig. 1.

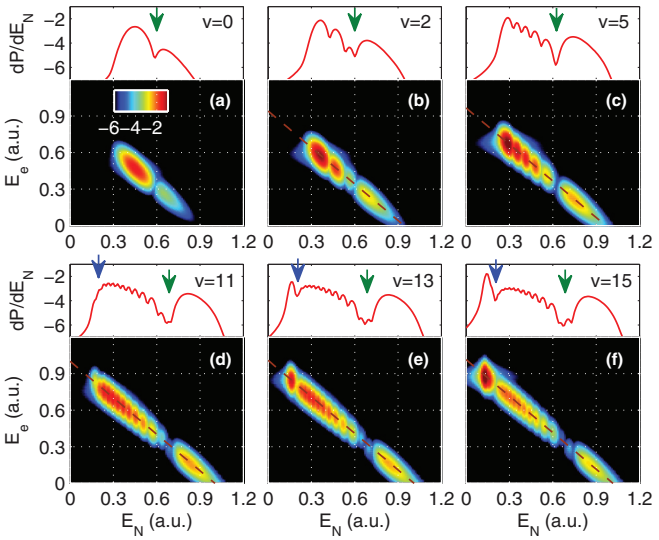

FIG. 1. (Color online) The JES (bottom panels) along with the KER spectra (top panels) for the interaction of the vibrational H_2^+ with a 0.8-fs XUV pulse at 30 nm and a peak intensity of 10^{14} W/cm^2. The color scaling is logarithmic.

From Fig. 1, several features of the spectra can be found. The first feature, as indicated by the dashed lines, is the maxima of the JES along the lines given by

$$E_N + E_e = E_{sys}(v) + \omega, \quad (2)$$

with E_N and E_e being the energy of correlated nuclei and electron, ω being the photon energy, and $E_{sys}(v)$ being the bound energy of the initial wave packets for the vth vibrational state. Obviously, this feature is governed by the energy conservation. For the details of energy sharing, however, one would need the specific expressions for E_N and E_e, which will be deduced later. The second feature is that there are more maxima in the JES for higher vibrational states. By integrating the JES over E_e, we show the KER spectra (red curves) in the top panels of Fig. 1. It is shown that the modulation of the KER spectra emerges in the single-photon absorption. Third, the pronounced suppressions are observed, as indicated by the arrows in Fig. 1. Furthermore, we show the kinetic-energy spectra of the nuclei and the electron for vibrational states from $v = 0$ to 16 in Figs. 2(a) and 2(b), respectively. As

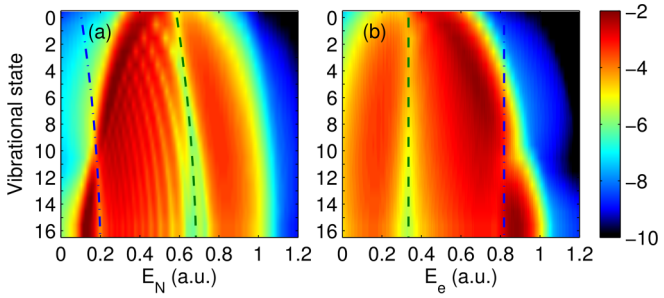

FIG. 2. (Color online) The kinetic-energy spectra of (a) the nuclei and (b) the electron for vibrational states from $v = 0$ to 16. The dashed and dash-dotted lines indicate the locations of the suppression. The color scaling is logarithmic.

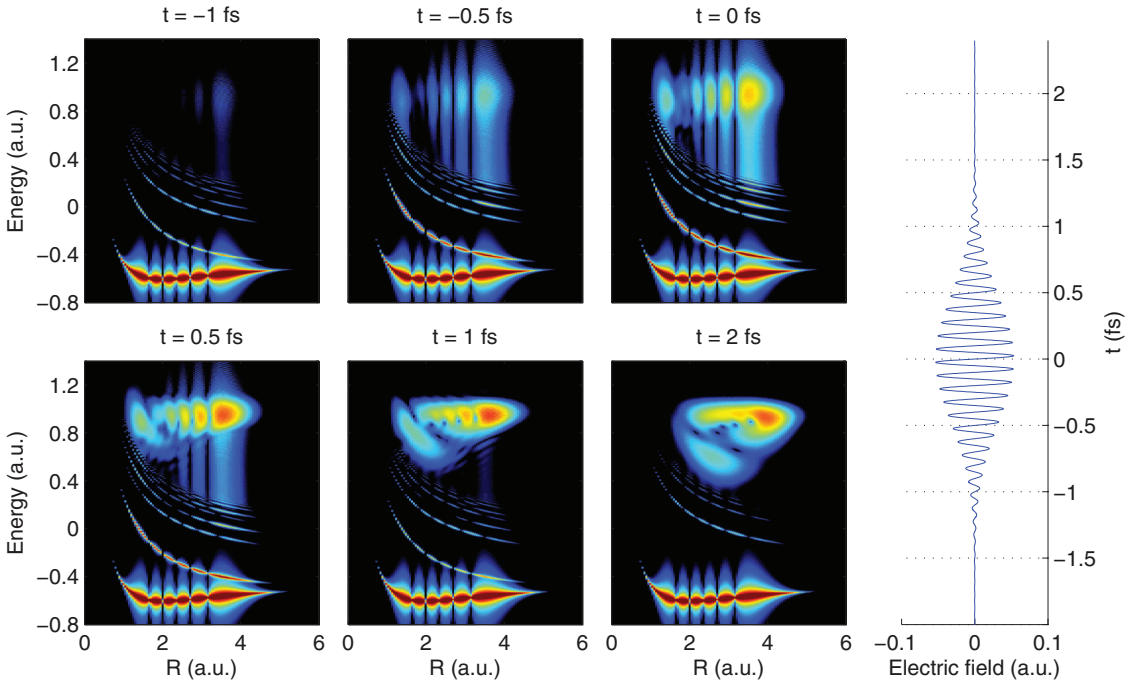

FIG. 3. (Color online) (left) Snapshots of the evolution of the EPI for the interaction of H_2^+ ($1s\sigma_g$, $v = 5$) with (right) the XUV pulse. The color scaling is logarithmic.

indicated by the dashed and dash-dotted lines, the locations of the suppressions in KER spectra shift to higher energy for higher vibrational states, while those in electronic energy spectra are independent of the initial states.

To find out the origins of the progression of the JES, we have simulated the evolution of the EPI for the interaction of H_2^+ ($1s\sigma_g$, $v = 5$) with the XUV pulse (see the multimedia movie in the Supplemental Material [33]). Each frame of the evolution is calculated at every half optical cycle when $\varepsilon(t) = 0$. Figure 3 shows the snapshots of the evolution of the EPI at several times and the corresponding electric field (right panel). In the EPIs, the bound population appears to spread in the energy direction. This is associated with the window width 2ϵ in the energy window operator. In our simulation, the spread of the bound population would decrease with ϵ, whereas the distribution of continuum population does not change significantly. In addition, from the EPIs one can see that a partial population remains in some excited states throughout the interaction. Such a population is due to the present numerical model of H_2^+. However, the magnitude of the population is several orders smaller than that in the ground state, and it has little influence on the observation of the population transfer from the ground state to the continuum during the interaction.

By following the time-dependent EPIs in Fig. 3, one can intuitively observe how the population is transferred during the interaction. In order to quantitatively discuss the interaction process, in Figs. 4(a) and 4(b) we show the EPIs at $t = 0$ and 1.5 fs, respectively, with the $1s\sigma_g$ potential curve $V_g(R)$ [the thick red (gray) one] and the $1/R$ Coulomb explosion curve (the thick white one) on them. In addition, the profile of the initial nuclear wave packets on the upshifted potential curve $V_g(R) + \omega$ [the thin red (gray) one] is shown in Fig. 4(a). As indicated by the thick yellow arrows in Figs. 4(a) and 4(b), the interaction process can be described as follows. First, the system absorbs one-photon energy, and the partial bound population is vertically transferred to the continuum with maxima along the $V_g(R) + \omega$ curve. Note that the region

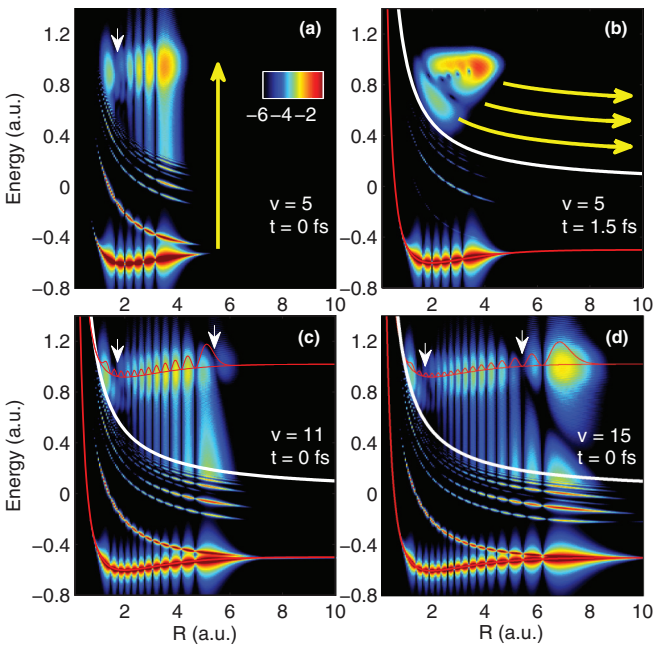

FIG. 4. (Color online) The EPIs during the interaction. The vibrational state and the time for each EPI have been given in the corresponding panel. The thick red (gray) and white curves indicate the $1s\sigma_g$ potential and the $1/R$ curves. The thin red (gray) curves denote the upshifted potential of $1s\sigma_g + \omega$ and the profile of the initial nuclear wave-packet distributions. The color scaling is logarithmic.

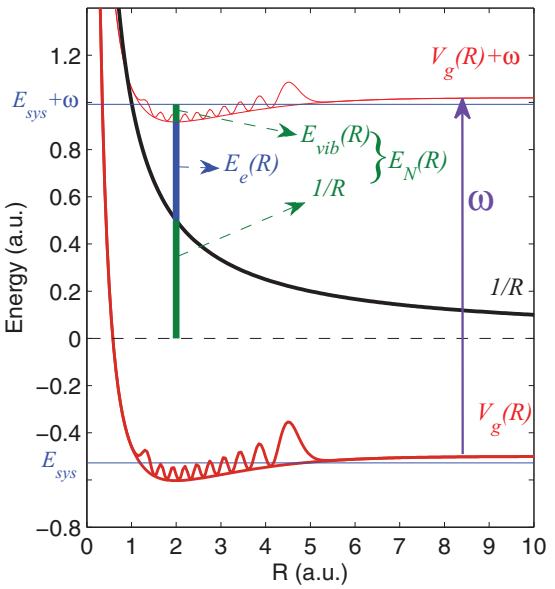

FIG. 5. (Color online) Illustration of electron-nuclear energy sharing in single-photon-induced dissociative ionization of H_2^+.

above the $1/R$ curve denotes the continuum electron states of all symmetries at each energy; thus, the bound population at each internuclear distance could be transferred to the region of the continuum as long as the absorbed photon energy is high enough for the population to overcome the $1/R$ curve. Then, the population at each R slides down along the respective routes parallel to the $1/R$ curve and moves to a large internuclear distance.

Based on the interaction process above, we now deduce the details of the energy sharing between the electron and the nuclei in Fig. 5. Assuming that the population is transferred from the $1s\sigma_g$ electronic state by absorbing the photon energy of ω, the centers of the continuum population at each R would be at the positions given by $E(R) = \omega + V_g(R)$. For the electron, the ponderomotive energy is close to zero due to the ultrashort wavelength of the XUV pulse. Thus, the electronic energy will stay constant after the transfer. Then the final electronic kinetic energy E_e as a function of R is given by

$$E_e(R) = E(R) - 1/R = \omega + V_g(R) - 1/R, \qquad (3)$$

where $1/R$ indicates the ionization threshold at each internuclear distance of R. For the nuclei, according to Eqs. (2) and (3), we deduce that the final nuclear kinetic energy is given by

$$E_N(R) = E_{sys}(v) - V_g(R) + 1/R = E_{vib}(R) + 1/R, \qquad (4)$$

where $E_{vib}(R) = E_{sys}(v) - V_g(R)$ denotes the vibrational energy of the nuclei at R when the Coulomb explosion starts. This confirms that the final nuclear kinetic energy includes the initial vibrational energy and the energy that arises from the Coulomb explosion.

The EPI in Fig. 4(a) also shows that the population being transferred to the continuum is proportional to the bound population and is suppressed at the internuclear distance indicated by the small arrow. This has been confirmed via the EPIs for other vibrational states shown in Figs. 4(c) and 4(d). The yields of the correlated electron (with energy E_e) and nuclei (with energy E_N) are thus

$$Y[E_N(R), E_e(R)] \propto |\chi(R)|^2 \Gamma(R) \qquad (5)$$

with $\chi_v(R)$ being the nuclear wave function of the vth vibrational state and $\Gamma(R)$ being the ionization rate at R. Generally, the energy-sharing rule given by Eqs. (3) and (4), together with Eq. (9), indicates that the yields of the correlated fragments at different energies are (i) determined by the R-distributed population and (ii) affected by the ionization rates at different R.

With Eqs. (3)–(5), now the spectral features in Figs. 1 and 2 can be well understood. On the one hand, because there are more peaks in the nuclear wave-packet distribution of higher vibrational states, more maxima appeared in the KER spectra and the JES, as shown in Fig. 1 and Fig. 2(a). The peaks in electronic energy spectra in Fig. 2(b) are blurred due to the broadband photon energy of ω in Eq. (3). On the other hand, from the EPIs in Figs. 4(a), 4(c), and 4(d), the positions of the suppression can be approximately read as $R_s \approx 1.70$ and 5.45 a.u. According to previous studies on the electronic wave-packet interference [34,35], the ionization would be suppressed at critical internuclear distances due to the destructive interference of the ionized electronic wave packets from two nuclei. The suppression happens whenever $pR = (2j-1)\pi$, with $j = 1,2,3,\ldots$ Here, p is the electron momentum when the electron is ejected from the nuclei. In single-photon ionization, the initial kinetic energy of the ejected electron is approximately equal to the photon energy ω. Then the value of R_s can be estimated by

$$R_s \approx (2j-1)\pi/\sqrt{2\omega}\,. \qquad (6)$$

Therefore, R_s is dependent on the wavelength. In our calculation, $\omega \approx 1.5198$ a.u., and we can obtain $R_s \approx 1.8019$ ($j = 1$) and 5.4058 ($j = 2$) a.u., which are close to the values obtained from the EPIs. The positions of the suppression in the EPIs are not exactly equal to the values given by Eq. (6) because they are also influenced by the nuclear wave-packet distribution. According to Eq. (5), the locations of the suppressions in the nuclear and electronic kinetic-energy spectra can be obtained by inserting R_s into Eqs. (3) and (4), respectively. Clearly, for a given R_s, $E_N(R_s)$ will increase with the bound energy of $E_{sys}(v)$, while $E_e(R_s)$ is independent of the vibrational state. We show the suppression locations, given by $E_N(R_s)$ and $E_e(R_s)$, with the dashed and dash-dotted lines in Fig. 2, and they are accurately consistent with the tendency of the suppression in the spectra.

Basically, the physical picture for the single-photon ionization of H_2^+ demonstrated by the EPI could be generalized to multiphoton and tunneling regimes. In Fig. 6, we show the EPIs (top row) for the interaction of H_2^+ ($1s\sigma_g$, $v = 15$) with the 400- and 800-nm pulses at $t = 0$ fs and the corresponding JES (bottom row). The pulse duration is three optical cycles, and the intensity is 10^{14} W/cm^2. The values of the Keldysh parameter for Figs. 6(a) and 6(b) are 2.52 and 1.26, respectively, corresponding to the ionization processes in multiphoton regimes and close to tunneling regimes [36]. Here, we double the calculation grid to ensure no significant

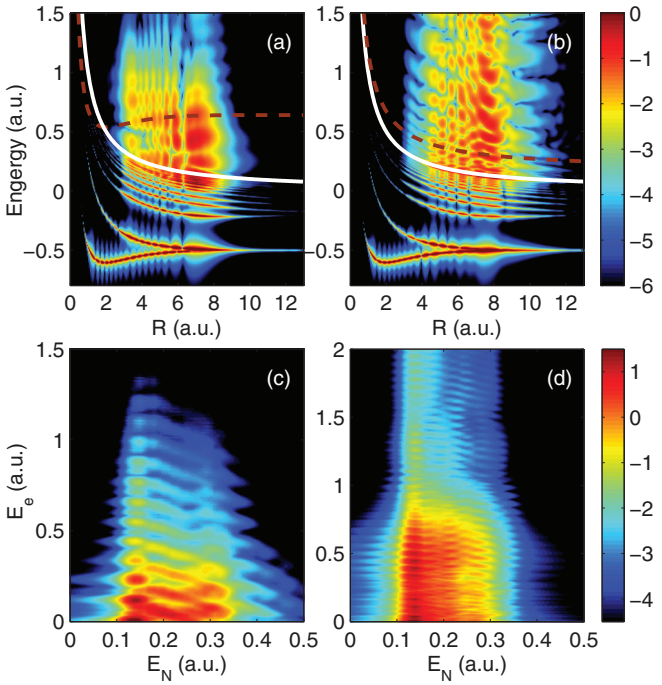

FIG. 6. (Color online) (a) and (b) The EPIs at $t = 0$ fs and (c) and (d) the JES for the interactions of H_2^+ ($1s\sigma_g$, $v = 15$) with (left) 400- and (right) 800-nm pulses. The pulse duration is three optical cycles, and the intensity is 10^{14} W/cm^2. The white solid curves indicate the $1/R$ curve. The dashed curves in (a) and (b) are the schematic lines, which are the vertically shifted $1s\sigma_g$ energy curve and $1/R$ curve, respectively. The color scaling is logarithmic.

reflection of the wave packets at the boundary during the interaction.

The EPIs in Figs. 6(a) and 6(b) demonstrate the coexistence of two somewhat controversial mechanisms: above-threshold Coulomb explosion [15] and charge-resonance-enhanced ionization [16]. First, the *vertical* arrangement of the maxima in the continuum is observed, intuitively verifying the multiphoton absorption process. Meanwhile, strong coupling between the $1s\sigma_g$ and $2p\sigma_u$ states is observed in the range of $3 < R < 8$ a.u., where the continuum population is much more pronounced than that of a small internuclear distance. The modulated population in bound states thus leads to the nearly *horizontal* arrangement of the maxima in the continuum. According to energy-sharing mechanism illustrated in Fig. 5 and the energy-sharing rule given by Eqs. (3) and (4), the maxima of each vertical column in the continuum will contribute to the multipeak structure of the electronic energy spectrum, while the nearly horizontal arrangement of the maxima is responsible for the modulated structure of the KER spectrum.

Furthermore, as illustrated by the dashed lines in Figs. 6(a) and 6(b), there are distinct horizontal arrangements of the maxima in the continuum, which are associated with the ionization processes. In the multiphoton regime [Fig. 6(a)], the bound population is "vertically" transferred to the continuum via multiphoton absorption [37], resulting in the population maxima along the upshifted $1s\sigma_g$ potential. Thus, similar to Eqs. (3) and (4), the energy sharing in the multiphoton regime can be roughly given by $E'_e(R) \approx n\omega' + V_g(R) - 1/R$ and $E'_N(R) \approx 1/R + E'_{vib}(R)$, which indicate that E'_e and E'_N are correlated through the parameter R, resulting in the tilted spectral structure in Fig. 6(c). In the tunneling regime [Fig. 6(b)], the bound population would first "tunnel" to the continuum and then absorb energy from the field [37]. As a result, the population maxima are almost along the lines parallel to the $1/R$ curve. Therefore, the energy sharing in the tunneling regime can be roughly given by $E''_e(R) \approx m\omega''$ and $E''_N(R) \approx 1/R + E''_{vib}(R)$, where E''_e is independent of the parameter R and thus loses the correlation with E''_N, as the JES shows in Fig. 6(d).

IV. SUMMARY

In summary, an intuitive representation, i.e., energy-resolved population imaging, was introduced to make the instantaneous molecular dynamics visible in a quantitative way. The population transfer and the details of the energy-sharing processes during dissociative ionization of H_2^+ have been intuitively demonstrated by the EPIs. Our results have clarified (i) that the electron-nuclear energy sharing is determined by the internuclear distance, vibrational energy of the nuclei, and photon energy and (ii) that the yields of the correlated fragments are associated with the nuclear wave-packet distribution and ionization rates at different internuclear distances. Moreover, on the basis of the EPIs, the different energy-sharing mechanisms in multiphoton and tunnel ionization of H_2^+ are found to originate from the distinct ways in which the bound population is transferred to the continuum.

The EPI in the present work suggests an alternative tool to analyze the dynamics of small molecules in strong field, and it would be helpful to explore the underlying molecular mechanisms in future experimental studies. In addition, by using EPI we will be able to obtain deeper insights into the correlated electron-nuclear dynamics not only in H_2^+ but also in more complex molecules like the neutral molecule H_2 and the asymmetric molecular ion HeH^{2+} as their TDSEs beyond Born-Oppenheimer approximation have already been solved [38,39].

ACKNOWLEDGMENTS

This work was supported by the National Natural Science Foundation of China under Grants No. 61275126 and No. 11234004 and the 973 Program of China under Grant No. 2011CB808103. Numerical simulations presented in this paper were carried out using the High Performance Computing Center experimental testbed in SCTS/CGCL (see http://grid.hust.edu.cn/hpcc).

[1] R. Velotta, N. Hay, M. B. Mason, M. Castillejo, and J. P. Marangos, Phys. Rev. Lett. **87**, 183901 (2001).

[2] A. D. Bandrauk, S. Chelkowski, S. Kawai, and H. Lu, Phys. Rev. Lett. **101**, 153901 (2008).

[3] M. Lein, Phys. Rev. Lett. **94**, 053004 (2005).
[4] S. Baker, J. S. Robinson, C. A. Haworth, H. Teng, R. A. Smith, C. C. Chirilă, M. Lein, J. W. G. Tisch, and J. P. Marangos, Science **312**, 424 (2006).
[5] C. D. Lin, A. Le, Z. Chen, T. Morishita, and R. Lucchese, J. Phys. B **43**, 122001 (2010).
[6] V. Roudnev, B. D. Esry, and I. Ben-Itzhak, Phys. Rev. Lett. **93**, 163601 (2004).
[7] M. F. Kling, C. Siedschlag, A. J. Verhoef, J. I. Khan, M. Schultze, T. Uphues, Y. Ni, M. Uiberacker, M. Drescher, F. Krausz, and M. J. J. Vrakking, Science **312**, 246 (2006).
[8] T. Zuo and A. D. Bandrauk, Phys. Rev. A **52**, R2511 (1995).
[9] T. Seideman, M. Y. Ivanov, and P. B. Corkum, Phys. Rev. Lett. **75**, 2819 (1995).
[10] F. He, A. Becker, and U. Thumm, Phys. Rev. Lett. **101**, 213002 (2008).
[11] N. Takemoto and A. Becker, Phys. Rev. Lett. **105**, 203004 (2010).
[12] J. H. Posthumus, Rep. Prog. Phys. **67**, 623 (2004).
[13] A. D. Bandrauk and M. L. Sink, J. Chem. Phys. **74**, 1110 (1981).
[14] A. Giusti-Suzor, X. He, O. Atabek, and F. H. Mies, Phys. Rev. Lett. **64**, 515 (1990).
[15] B. D. Esry, A. M. Sayler, P. Q. Wang, K. D. Carnes, and I. Ben-Itzhak, Phys. Rev. Lett. **97**, 013003 (2006).
[16] A. Staudte, D. Pavičić, S. Chelkowski, D. Zeidler, M. Meckel, H. Niikura, M. Schöffler, S. Schössler, B. Ulrich, P. P. Rajeev, T. Weber, T. Jahnke, D. M. Villeneuve, A. D. Bandrauk, C. L. Cocke, P. B. Corkum, and R. Dörner, Phys. Rev. Lett. **98**, 073003 (2007).
[17] S. Chelkowski, A. D. Bandrauk, A. Staudte, and P. B. Corkum, Phys. Rev. A **76**, 013405 (2007).
[18] H. A. Leth, L. B. Madsen, and K. Mølmer, Phys. Rev. A **81**, 053410 (2010).
[19] B. D. Esry and I. Ben-Itzhak, Phys. Rev. A **82**, 043409 (2010).
[20] A. Kiess, D. Pavičić, T. W. Hänsch, and H. Figger, Phys. Rev. A **77**, 053401 (2008).
[21] X. Chu, Phys. Rev. A **78**, 043408 (2008).
[22] M. Winter, R. Schmidt, and U. Thumm, Phys. Rev. A **80**, 031401(R) (2009).
[23] H. A. Leth, L. B. Madsen, and K. Mølmer, Phys. Rev. Lett. **103**, 183601 (2009).
[24] F. Sami, M. Vafaee, and B. Shokri, J. Phys. B **44**, 165601 (2011).
[25] C. B. Madsen, F. Anis, L. B. Madsen, and B. D. Esry, Phys. Rev. Lett. **109**, 163003 (2012).
[26] R. E. F. Silva, F. Catoire, P. Rivière, H. Bachau, and F. Martín, Phys. Rev. Lett. **110**, 113001 (2013).
[27] A. Fischer, A. Sperl, P. Cörlin, M. Schönwald, H. Rietz, A. Palacios, A. González-Castrillo, F. Martín, T. Pfeifer, J. Ullrich, A. Senftleben, and R. Moshammer, Phys. Rev. Lett. **110**, 213002 (2013).
[28] J. Wu, M. Kunitski, M. Pitzer, F. Trinter, L. P. H. Schmidt, T. Jahnke, M. Magrakvelidze, C. B. Madsen, L. B. Madsen, U. Thumm, and R. Dörner, Phys. Rev. Lett. **111**, 023002 (2013).
[29] K. C. Kulander, F. H. Mies, and K. J. Schafer, Phys. Rev. A **53**, 2562 (1996).
[30] B. Feuerstein and U. Thumm, Phys. Rev. A **67**, 043405 (2003).
[31] K. Liu, W. Hong, Q. Zhang, and P. Lu, Opt. Express **19**, 26359 (2011).
[32] K. J. Schafer and K. C. Kulander, Phys. Rev. A **42**, 5794 (1990).
[33] See Supplemental Material at http://link.aps.org/supplemental/10.1103/PhysRevA.89.053423 for the movie of the evolution of the EPI for the interaction of $H_2^+(1s\sigma_g, v = 5)$ with the XUV pulse.
[34] C. Huang, Y. Zhou, Q. Liao, and P. Lu, J. Opt. Soc. Am. B **29**, 734 (2012).
[35] J. Henkel, M. Lein, and V. Engel, Phys. Rev. A **83**, 051401(R) (2011).
[36] P. Eckle, A. N. Pfeifer, C. Cirelli, A. Staudte, R. Dörner, H. G. Muller, M. Büttiker, and U. Keller, Science **322**, 1525 (2008).
[37] M. Y. Ivanov, M. Spanner, and O. Smirnova, J. Mod. Opt. **52**, 165 (2005).
[38] J. L. Sanz-Vicario, H. Bachau, and F. Martín, Phys. Rev. A **73**, 033410 (2006).
[39] K. Liu, W. Hong, and P. Lu, Opt. Express **19**, 20279 (2011).